Enantiospecificity of Cysteine Adsorption on a Ferromagnetic Surface: Is it Kinetically or Thermodynamically Controlled?

Y. Lu, B. P. Bloom, S. Qian, and D. H. Waldeck*

Chemistry Department, University of Pittsburgh, Pittsburgh PA 15260

Corresponding Author Email: dave@pitt.edu

(412) 624-8430

Keywords: CISS, enantiomer resolution, cysteine, EQCM, chirality

Abstract: This work uses electrochemical quartz crystal microbalance methods to demonstrate the enantiospecific interaction between a magnetized surface and a chiral amino acid. The enantiospecific adsorption of chiral molecules (cysteine is used as a model) on a ferromagnetic surface is shown to arise from the kinetics of adsorption and not from a thermodynamic stabilization. Measurements of the Gibbs free energy of adsorption for different chiral forms of cysteine and different electrode magnetization states show no significant differences, whereas measurements of the adsorption and desorption kinetics reveal a strong dependence on the magnetization state of the electrode surface. In addition, the enantioselectivity is shown to depend sensitively on the solution pH and the charge state of the chiral adsorbate.

TOC Graphic

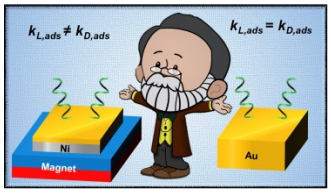

Enantiopurity has been long known to affect the efficacy of pharmaceuticals[1] as well as chemical agents in other applications, such as agriculture.[2] This fact has driven the development of methods for chiral resolution including an array of chromatographic techniques and the crystallization of diastereomeric salts.[3,4,5] A recent study by Banerjee-Ghosh *et al.*[6] showed that magnetized metal surfaces could be used to resolve a racemic solution of oligopeptides in a flow cell, for which the elution time of the oligopeptide depends on the magnetization direction of the magnetized surface and the handedness of the enantiomer. The enantiospecific interaction of a chiral molecule with a magnetic substrate originates from the chiral induced spin selectivity (CISS) effect.[7,8,9] Because charge polarization of a chiral molecule's electron cloud is accompanied by a spin polarization,[10] an enantiospecific preference manifests when the spin polarized chiral molecule is aligned favorably with that of the magnetized substrate. In a racemic solution, the two enantiomers exhibit opposite spin polarizations upon charge polarization and hence interact

differently with a magnetized surface. Later extensions of this phenomenon demonstrated enantioselective electrochemical reduction (and oxidation) of a racemate,[11,12] the generation of pure conglomerates,[13,14] and rate-dependent polymerization[15] on magnetized surfaces. Collectively, these studies illustrate that magnetic substrates and chiral molecules exhibit enantiospecific interactions which may be useful for enantioselective separation and synthesis.

Despite the remarkable proof-of-concept shown using CISS for enantiomeric resolution, a greater fundamental understanding of the principles which govern enantiospecificity at magnetic interfaces is required to assess the potential of this technique for real-world applications. This study uses an electrochemical quartz crystal microbalance (EQCM) method to examine whether the enantiospecific adsorption of the chiral amino acid cysteine on a magnetized ferromagnetic substrate arises from kinetic differences or thermodynamic ones. Moreover, these studies demonstrate that the adsorption process is the determining factor for successful enantioselectivity and show that the enantiospecificity is sensitive to the molecular orientation and ionization state of the cysteine.

A scheme of the EQCM experimental method is shown in Figure 1a. The EQCM monitors the resonant frequency of a quartz crystal, which is coated with a metal film (100 nm Ni/10 nm Au) electrode, to quantify the adsorption and desorption of cysteine on the electrode surface as a function of electrode potential (and time).[16] During the experiment a 0.54 T magnet was used to magnetize the Ni film electrode; North (South) denotes which magnetic pole is pointing toward the electrolyte and normal to the Ni film surface (see SI for more details). Figure 1b shows EQCM data for a 1 μg/mL solution of L-cysteine in a pH 8 phosphate buffer. The top panel of 1b shows a cyclic voltammogram and the bottom panel shows the corresponding frequency change of the quartz crystal. In order to ensure that the system reached steady-state, the cell was allowed to equilibrate for one hour prior to measurements; and the data in Figure 1b are from the 30th voltage cycle after equilibration. Scanning the voltage cathodically reveals a current peak at -0.8 V and a concomitant frequency increase that correspond to the reductive desorption of L-cysteine from the electrode surface. A subsequent anodic voltage scan reveals a broad current peak and concomitant decrease in the QCM frequency, which arise from the oxidative adsorption of L-cysteine onto the electrode. A similar behavior for alkanethiols on gold using EQCM was shown previously[17,18] and similar potentials were observed for the desorption of cysteine using cyclic voltammetry.[24] A frequency shift of -1.0 Hz corresponds to a mass change of 1.4 ng, or $\sim 7 \times 10^{12}$ cysteine molecules. Combining the frequency change in Figure 1b with an electrode area of 0.205 cm^2 gives a surface coverage of 2.5×10^{-10} mol / cm^2, or ~ 65 Å^2 per molecule, a value close to that for a full monolayer.

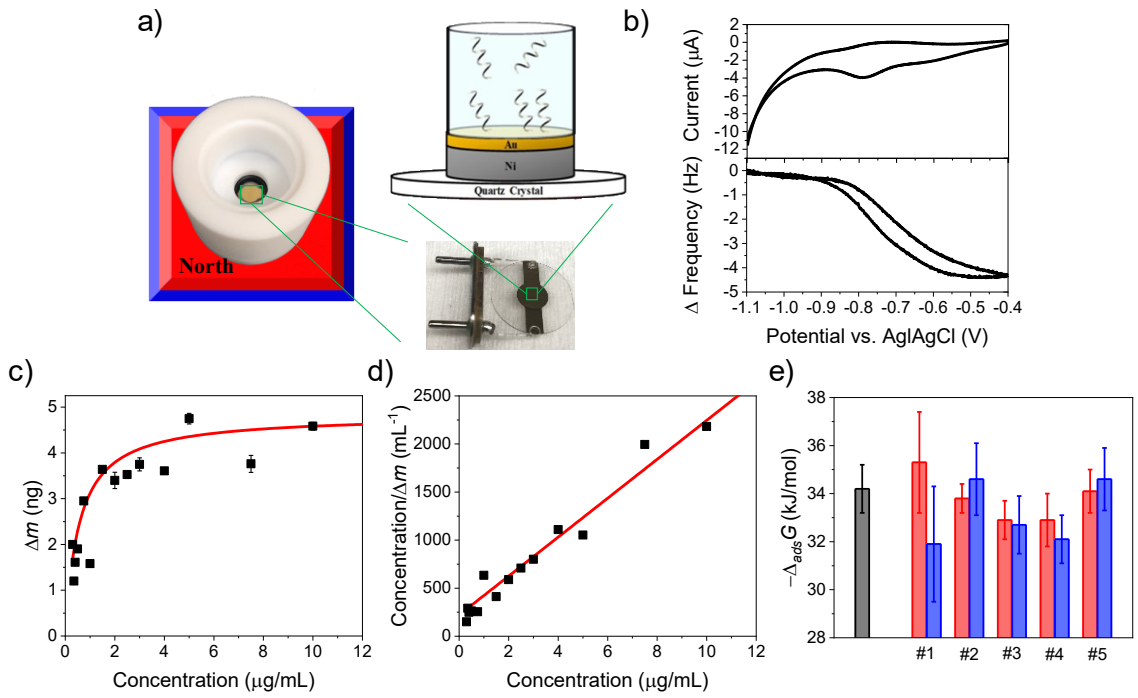

Figure 1. Panel a) shows an image and scheme for the electrochemical quartz crystal microbalance (EQCM) measurements. A custom-made quartz crystal electrode (100 nm Ni /10 nm Au), which is magnetized by a permanent magnet, was used to monitor the adsorption of cysteine from solution. Panel b) shows a cyclic voltammogram (top) and corresponding frequency change (bottom) for the electrode in contact with a 10 μg/mL L-cysteine solution in pH 8 phosphate-buffer. Panel c) shows an adsorption isotherm of L-cysteine using the change in mass, Δm, from the EQCM measurements at different cysteine concentrations. The red line is a Langmuir isotherm fit to the data. Panel d) shows a linearized form of the data in panel c (the r correlation coefficient is 0.92). Panel e) shows a histogram of the calculated $\Delta_{ads}G$ for different EQCM electrodes (#1 through #5) under North (red) and South (blue) applied magnetic field. Studies without a magnetic field on an Au electrode are shown in black. The error bars are associated with error in the linearized isotherm fit (see SI for details).

To elucidate the effect of Ni magnetization on the thermodynamics of cysteine adsorption, the change in mass, Δm, as a function of cysteine concentration, c_{cys}, from 0.25 μg/mL to 10 μg/mL, was monitored in a pH 8 phosphate buffer; see Figure 1c and d. The data were fit by a Langmuir adsorption model[19,20] to obtain a value of $\Delta_{ads}G$ (see the SI for more detail). For $c_{cys} > 5$ μg/mL the surface coverage of cysteine is largely saturated, ~2.5×10-[10] mol / cm^2, and constitutes monolayer formation.[24] Figure 1e shows a histogram plot of $\Delta_{ads}G$ for L-cysteine on different electrodes for different magnetization conditions; the height of the histogram gives the $\Delta_{ads}G$ values and the abscissa lists the trials using different EQCM electrodes. Note, the ordinate scale is expanded to make the error and variation in $\Delta_{ads}G$ more apparent. The average $\Delta_{ads}G$ for North (red) and South (blue) applied magnetization across the multiple trials is -33.8 ± 1.1 kJ/mol and -33.2 ± 1.5 kJ/mol, respectively. The $\Delta_{ads}G$ values determined under an applied magnetic field are in reasonable agreement with that on a nonmagnetic Au electrode (black, -34.2 ± 1.0 kJ/mol) and consistent with other literature reports.[21,22] These data indicate that the magnetic field orientation does not significantly change the $\Delta_{ads}G$ for L-cysteine. Similar experiments were

performed for D-cysteine and found to be within error to those of L-cysteine; see Supplementary Information. Thus, the adsorption equilibrium does not change significantly with the molecules' handedness (D- versus L-forms) or the substrate magnetization direction. Lastly, this 'null' result demonstrates that the Au surface does not have an intrinsic chiral bias.

Time-dependent QCM measurements, for different magnetization conditions of the electrode, were used to monitor the desorption and adsorption kinetics of cysteine. Based on the voltammogram (Figure 1b), the applied potential for desorption was set to be -0.8 V or more and that for adsorption of cysteine was set to be -0.5 V. The applied voltage was jumped between these two values and the QCM response was collected as a function of time after the potential jump. Small deviations from the set potentials caused little to no change in the time response. Figure 2 shows the observed QCM frequency response (black) upon application of the described voltage sequence (blue). A total of 150 cycles at the two different applied potentials was acquired and the QCM response for each 5 s time period were fit by an exponential profile to obtain the adsorption and desorption rate constants; see SI for details. The fits to the desorption transient signals provide the desorption rate constant k_{des} directly; and the fits to the adsorption transients provide the effective adsorption rate constant k'_{ads}, which is given by $k'_{ads} = k_{ads} \cdot c_{cys}$ where k_{ads} is the adsorption rate constant (see SI for more discussion). Figure 2 (right) shows histograms of k_{des} (top) and k'_{ads} (bottom) of a 1 µg/mL D-cysteine solution with a North (red) and South (blue) applied magnetic field. The bin size for the histograms is 0.1 s^{-1} for desorption and 0.05 s^{-1} for adsorption. The histograms were fit by a Gaussian distribution to obtain the average and standard deviation of the mean rate constant (values are reported in Table S1). A significant dependence on the magnetization is observed for the D-cysteine adsorption at the -0.5V bias, the adsorption rate is higher for a South magnetized electrode than for a North magnetized electrode. The desorption process (measured at -0.8 V bias) also shows a dependence on the magnetization, however the difference is harder to resolve because of the time resolution of the measurement.

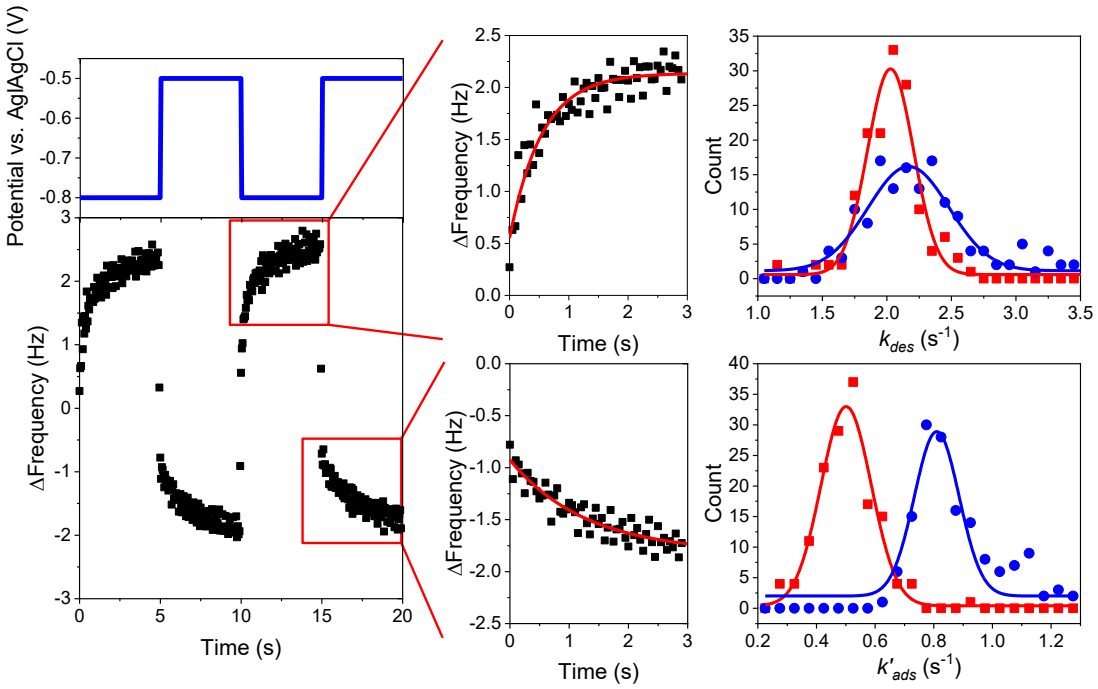

Figure 2. Chronoamperometry data (left) for a 1 μg/mL solution of D-cysteine. The applied potentials are shown in blue (top) and the frequency response is shown in black (bottom). The middle graphs show an expanded plot of the desorption (top) and adsorption (bottom) fits by an exponential decay or growth (red line) for determining the rate constant. The histograms on the right comprise >150 fits of the desorption (top) and adsorption (bottom) processes under a North magnetic field (red) and South magnetic field (blue). A best fit of the data using a Gaussian distribution is shown as a solid line.

The adsorption kinetics of D-cysteine and L-cysteine were studied at a series of different concentrations from 1 μg/mL to 5 μg/mL (see Table S1 and Figure S3). The adsorption rate for L-cysteine displays a faster effective rate constant under North magnetization than it does under South magnetization, whereas the reverse is true for D-cysteine. The asymmetry in the adsorption rates and the inverse behavior of the enantiomers is consistent with a CISS mediated effect.[9] To quantify the asymmetry, we define a polarization parameter, P as

$$P = \frac{k'_{ads,N} - k'_{ads,S}}{k'_{ads,N} + k'_{ads,S}} \cdot 100\%$$

Note that P corresponds closely to an enantiomeric excess *ee* for the adsorption process. Figure 3 plots the experimentally determined P values as a function of L-cysteine (green) and D-cysteine (purple) concentration in Figure 3. Measurements with the achiral molecule mercaptopropionic acid (black) in solution gives a zero polarization. For L-cysteine, the polarization reaches a maximum value of 33% at 1 μg/mL and decreases to 4.6% at 5 μg/mL, whereas for D-cysteine the polarization is maximum at 1 μg/mL (-24 %) and decreases to ~-2.3% at 5 μg/mL. Solution concentrations of cysteine below 1 μg/mL resulted in mass changes that were too noisy to accurately fit and obtain kinetic information. These data demonstrate that the adsorption rate of D-cysteine and L-cysteine onto a ferromagnetic substrate depends on the magnetic field direction and the molecular handedness at low concentrations, however as the concentration of cysteine in the solution increases, the polarization in the adsorption kinetics decreases and becomes hard to discern. Assuming that the adsorption mechanism is not changing with concentration, the decrease in polarization with increasing concentration can originate from a dependence of the relaxation back to equilibrium on the concentration of cysteine in solution. That is, a faster approach to equilibrium, at which no chiral selectivity manifests (see Fig 1), results in a lower polarization to be observed in the measurement. These findings imply that the enantioseparation of racemates reported by Banerjee-Ghosh *et al.*[6] is likely to be kinetically controlled.

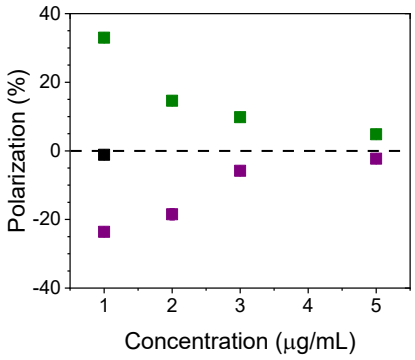

Figure 3. The polarization in adsorption rate constant for MPA (black), L-cysteine (green), and D-cysteine (purple) at different concentrations.

It is well known that solution conditions can affect cysteine's adsorption behavior. At intermediate pHs, where the zwitterionic form of cysteine exists, the binding geometry of cysteine has been shown to depend on the applied potential and scan rate; a process which changes under more acidic or basic conditions.[23,24] Cysteine can also dimerize to form cystine, a disulfide, in which the packing density and organization differ.[24] Also, Benesh *et al*. showed that the similar ionization constants for the nitrogen and sulfur moieties lead to charge isomerization.[25] Moreover, studies of chiral imprinting by organic ligands on nanoparticles have demonstrated that the handedness of the induced chirality can be strongly dependent on ligand packing and binding geometry.[26,27,28] In aggregate, these different phenomena illustrate the potential complexity of the substrate-cysteine interaction during adsorption, which could impact the observed P values; e.g., the molecular adsorption of cysteine rotamers[29,30] could give rise to opposite P values.

Figure 4 shows measurements of P for 1 μg/mL solutions of L-cysteine and L-cysteine methyl ester as a function of the solution pH. For cysteine (Fig 4a), P is large and positive at pH 8 (33%), but quickly transitions to a negative value as the pH increases to 8.56 (-15%) before asymptotically decreasing toward zero as the pH becomes large; see Table S2 for the rate constants. The crossover from positive to negative polarizations is concomitant with the $\mathrm{p}K_a = 8.3$ of the sulfur moiety of cysteine in solution[31] and suggests that the enantiospecificity is sensitive to the geometry and structure of the adsorbate. This inference is substantiated by the data for L-cysteine methyl ester which has a $\mathrm{p}K_a = 6.6$ for its thiol group.[31] Fig 4b, shows that P for the methyl ester form is strongly negative at pH 6.6, but increases to ~7% at pH 7 before falling asymptotically toward zero at pH 10. Interestingly, P for cysteine methyl ester is negative at low pH whereas P for cysteine itself is positive at low pH. We posit that the inverted behavior for cysteine and cysteine methyl ester at the thiol $\mathrm{p}K_a$ is rooted in the charge state of the adsorbate. Indeed, previous studies have shown that the charge polarization of a chiral molecule is linked to its CISS response.[10,32,33] While more elaborate studies of cysteine and its derivatives are required to better understand this effect, the pH studies illustrate the important role that solution conditions and adsorbate ionization state are likely to play for enantioseparations with magnetized surfaces.

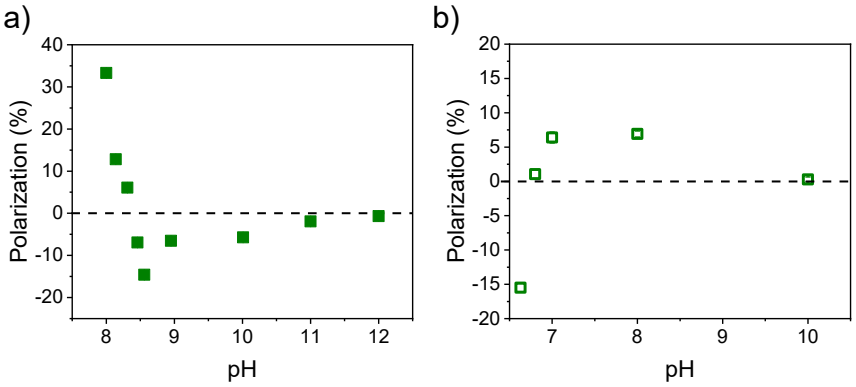

Figure 4. The polarization is plotted as a function of the solution pH for L-cysteine (panel a) and L-cysteine methyl ester (panel b).

This work shows that the enantiospecific interaction of cysteine with a magnetized ferromagnetic substrate is kinetically controlled and depends sensitively on the solution conditions (ionization state of the cysteine). Measurements of the adsorption isotherm show that the Gibbs

free energy of adsorption $\Delta_{ads}G$ on an Au coated ferromagnetic electrode does not change with the cysteine chirality or the electrode's magnetization state. In contrast, the kinetics for the adsorption (and desorption) show a significant dependence on the magnetic field direction and the handedness of the molecule. Concentration and pH studies of the adsorption polarization reveal the importance of molecular binding geometry for successful enantiomeric resolution.

Author Information

Corresponding Author

*E-mail: dave@pitt.edu Tel.: (412) 624-8430

Orcid

Brian P. Bloom: 0000-0001-9581-9710

David H. Waldeck: 0000-0003-2982-0929

Notes

The authors declare no competing financial interest.

Acknowledgements

This work was supported by the National Science Foundation (CBET 1852588).

Supplemental Text

EQCM details, UPD experiments, Adsorption Isotherm information, Linearization derivation of isotherm, Isotherm data for D-cysteine, Kinetic experimental details, experiments and model for derivation of kinetic information, Histogram data at different concentrations, relevant rate and polarization data for L-cysteine, D-cysteine, and L-cysteine methyl ester.

References

1 William, K.; Lee, E. Importance of drug enantiomers in clinical pharmacology *Drugs* **1985**, *30*, 333-354.

2 Garrison, A. W.; Schmitt-Kopplin, P.; Avants, J. K. Analysis of the Enantiomers of Chiral Pesticides and Other Pollutants in Environmental Samples by Capillary Electrophoresis. in *Capillary Electrophoresis: Methods and Protocols* (ed. Schmitt-Kopplin, P.) 157–170 (Humana Press, **2008**).

3 Nguyen, L. A.; He, H.; Pham-Huy, C. Chiral drugs: an overview. *Int. J. Biomed. Sci.* **2006**, *2*, 85-100.

4 Okamoto, Y.; Ikai, T. Chem. Chiral HPLC for efficient resolution of enantiomers. *Chem. Soc. Rev.* **2008**, *37*, 2593-2608.

5 Ward, T. J.; Ward, K. D. Chiral separations: fundamental review. *Anal. Chem.* **2010**, *82*, 4712-4722.

6 Banerjee-Ghosh, K.; Dor, O. B.; Tassinari, F.; Capua, E.; Yochelis, S.; Capua, A.; Yang, S.-H.; Parkin, S. S. P.; Sarkar, S.; Kronik, L.; Baczewski, L. T.; Naaman, R.; Paltiel, Y. Separation of enantiomers by their enantiospecific interaction with achiral magnetic substrates. *Science* **2018**, *360*, 1331-1334.
7 Naaman, R.; Paltiel, Y.; Waldeck, D. H. Chiral induced spin selectivity gives a new twist on spin-control in chemistry. *Acc. Chem. Res.* **2020**, *53*,2659-2667.
8 Naaman, R.; Paltiel, Y.; Waldeck, D. H. Chiral molecules and the spin selectivity effect. *J. Phys. Chem. Lett.* **2020**, *11*, 3660-3666.
9 Naaman, R.; Paltiel, Y.; Waldeck, D. H. Chiral molecules and the electron spin. *Nat. Rev. Chem.* **2019***, 3*, 250-260.
10 Ghosh, S.: Mishra, A.; Avigad, E.; Bloom, B. P.; Baczewski, L. T.; Yochelis, S.; Paltiel, Y.; Naaman, R.; Waldeck, D. H. Effect of Chiral Molecules on the Electron's Spin Wavefunction at Interfaces. *J. Phys. Chem. Lett.* **2020**, *11*, 1550-1557.
11 Bloom, B. P.; Lu, Y.; Metzger, T.; Yochelis, S.; Paltiel, Y.; Fontanesi, C.; Mishra, S.; Tassinari, F.; Naaman, R.; Waldeck, D. H. Asymmetric reactions induced by electron spin polarization. *Phys. Chem. Chem. Phys*., **2020**, *22*, 21570-21582.
12 Metzger, T. S.; Mishra S.; Bloom B. P.; Goren, N.; Neubauer, A.; Shmul, G.; Wei, J.; Yochelis, S.; Tassinari, F.; Fontanesi, C.; Waldeck, D. H.; Paltiel, Y.; Naaman, R. The Electron Spin as a Chiral Reagent. *Angew. Chem. Int. Ed.* **2020**, *59*, 1653-1658.
13 Tassinari, F.; Steidel, J.; Paltiel, Shahar, Fontanesi, C.; Lahav, M.; Paltiel, Y.; Naaman, R. Enantioseparation by crystallization using magnetic substrates. *Chem. Sci.* **2019**, *10*, 5246-5250.
14 Bhowmick, D.; Sang, Y.; Santra, K.; Halbauer, M.; Capua, E.; Paltiel, Y.; Naaman, R.; Tassinari, F. Simultaneous High-Purity Enantiomeric Resolution of Conglomerates Using Magnetic Substrates. *Cryst. Growth Des.* **2021**, *21*, 2925-2931.
15 Tassinari, F.; Amsallem, D.; Bloom, B. P.; Lu, Y.; Bedi, A.; Waldeck, D. H.; Gidron, O.; Naaman, R. Spin-Dependent Enantioselective Electropolymerization. *J. Phys. Chem. C* **2020**, *124*, 20974-20980.
16 King, W. H. Piezoelectric sorption detector. *Anal. Chem.* **1964**, *36*, 1735-1739.
17 Qu, D.; Morin M. An EQCM study of the oxidative deposition of alkylthiolates on gold. *J. Electroanal. Chem.* **2001**, *517*, 45-53.
18 Qu, D.; Morin M. The kinetics of the electroformation of a self-assembled monolayer of butanethiols on gold. *J. Electroanal. Chem.* **2002**, *524*, 77-80.
19 Adamson, A. W. *Physical Chemistry of Surfaces*, 5th edn Wiley[J]. New York, **1990**.
20 Swenson, H.; Stadie, N. P. Langmuir's theory of adsorption: A centennial review. *Langmuir* **2019,** *35*, 5409-5426.
21 Yang, W.; Gooding, J. J.; Hibbert, D. B. Characterisation of gold electrodes modified with self-assembled monolayers of L-cysteine for the adsorptive stripping analysis of copper. *J. Electroanal. Chem.* **2001**, *516*, 10-16.
22 Hager, G.; Brolo, A. G. Adsorption/desorption behaviour of cysteine and cystine in neutral and basic media: electrochemical evidence for differing thiol and disulfide adsorption to a Au(1 1 1) single crystal electrode. *J. Electroanal. Chem.* **2003**, *550*, 291-301.
23 Brolo, A. G.; Germain P.; Hager G. Investigation of the Adsorption of L-Cysteine on a Polycrystalline Silver Electrode by Surface-Enhanced Raman Scattering (SERS) and Surface-Enhanced Second Harmonic Generation (SESHG). *J. Phys. Chem. B*, **2002**, *106*, 5982-5987.
24 Hager, G.; Brolo, A. G. Protonation and deprotonation of cysteine and cystine monolayers probed by impedance spectroscopy. *J. Electroanal. Chem.* **2009**, *625*,109-116.
25 Benesch, R.E.; Benesch, R. The acid strength of the-SH group in cysteine and related compounds. *J. Am. Chem. Soc.* **1955**, *77*, 5877.
26 Kuznetsova, V. A.; Mates-Torres, E.; Prochukhan, N.; Marcastel, M.; Purcell-Milton, F.; O'Brien, J.; Visheratina, A. K.; Martinez-Carmona, M.; Gromaova, Y.; Garcia-Melchor, M.;

Gun'ko, Y. K. Effect of Chiral Ligand Concentration and Binding Mode on Chiroptical Activity of CdSe/CdS Quantum Dots. *ACS Nano* **2019**, *13*, 13560-13572.

27 Choi, J. K.; Haynie, B. E.; Tohgha, U.; Pap, L.; Elliott, K. W.; Leonard, B. M.; Dzyuba, S. V.; Varga, K.; Kubelka, J.; Balaz, M. Chirality inversion of CdSe and CdS quantum dots without changing the stereochemistry of the capping ligand. *ACS Nano* **2016**, *10*, 3809-3815.

28 Bloom, B. P.; Graff, B. M.; Ghosh, S.; Beratan, D. N.; Waldeck, D. H. Chirality control of electron transfer in quantum dot assemblies. *J. Am. Chem. Soc.* **2017**, *139*, 9038-9043.

29 Harding, M. M.; Long, H. A. The crystal and molecular structure of L-cysteine. *Acta Crystallogr., Sect. B* **1968**, *24*, 1096.

30 Noszal, B.; Visky, D.; Kraszni, M. Population, acid− base, and redox properties of N-acetylcysteine conformers. *J. Med. Chem.* **2000**, *43*, 2176-2182.

31 Burner, U.; Obinger, C. Transient-state and steady-state kinetics of the oxidation of aliphatic and aromatic thiols by horseradish peroxidase. *FEBS Lett.* **1997**, *411*,269-274.

32 Kumar, A.; Capua, E.; Kesharwani, M. K.; Martin, J. M. L.; Sitbon, E.; Waldeck, D. H.; Naaman, R. Chirality-induced spin polarization places symmetry constraints on biomolecular interactions. *Proc, Nat. Acad. Sci.* **2017**, *114*, 2474-2478.

33 Fransson, J. Charge Redistribution and Spin Polarization Driven by Correlation Induced Electron Exchange in Chiral Molecules. *Nano Lett.* **2021**, *21*, 3026-3032.